

## Partitioning of evapotranspiration and its controls in four grassland ecosystems: Application of a two-source model

Hu Zhongmin<sup>a,b</sup>, Yu Guirui<sup>a,\*</sup>, Zhou Yanlian<sup>c</sup>, Sun Xiaomin<sup>a</sup>, Li Yingnian<sup>d</sup>, Shi Peili<sup>a</sup>, Wang Yanfen<sup>b</sup>, Song Xia<sup>e</sup>, Zheng Zemei<sup>a,b</sup>, Zhang Li<sup>a</sup>, Li Shengong<sup>a</sup>

<sup>a</sup> Synthesis Research Center of Chinese Ecosystem Research Network, Key Laboratory of Ecosystem Network Observation and Modeling, Institute of Geographic Sciences and Natural Resources Research, Chinese Academy of Sciences, Beijing 100101, China

<sup>b</sup> Graduate University of Chinese Academy of Sciences, Beijing 100049, China

<sup>c</sup> School of Geographic and Oceanographic Sciences, Nanjing University, Nanjing 210093, China

<sup>d</sup> Northwest Institute of Plateau Biology, Chinese Academy of Sciences, Xining 810001, China

<sup>e</sup> Ecosystem Dynamics and Global Ecology Laboratory, School of Forestry and Wildlife Science, Auburn University, Auburn, AL 36849, USA

### ARTICLE INFO

#### Article history:

Received 14 December 2007

Received in revised form 23 March 2009

Accepted 25 March 2009

#### Keywords:

Canopy stomatal conductance

Evapotranspiration

Leaf area index

Shuttleworth–Wallace

Soil water evaporation

### ABSTRACT

Quantifying the partitioning of evapotranspiration (ET) and its controls are particularly important for accurate prediction of the climatic response of ecosystem carbon, water, and energy budgets. In this study, we employed the Shuttleworth–Wallace model to partition ET into soil water evaporation ( $E$ ) and vegetation transpiration ( $T$ ) at four grassland ecosystems in China. Two to three years (2003–2005) of continuous measurements of ET with the eddy covariance technique were used to test the long-term performance of the model. Monte Carlo simulations were performed to estimate the key parameters in the model and to evaluate the accuracy in model partitioning (i.e.  $E/ET$ ). Results indicated that the simulated ET at the four ecosystems was in good agreement with the measurements at both the diurnal and seasonal timescales, but the model tended to underestimate ET by 3–11% on rainy days, probably due to the lack of model representation of rainfall interception. In general,  $E$  accounted for a large proportion of ET at these grasslands. The monthly  $E/ET$  ranged from 12% to 56% in the peak growing seasons and the annual  $E/ET$  ranged from 51% to 67% across the four ecosystems. Canopy stomatal conductance controlled  $E/ET$  at the diurnal timescale, and the variations and magnitude of leaf area index (LAI) explained most of the seasonal, annual, and site-to-site variations in  $E/ET$ . A simple linear relationship between growing season LAI and  $E/ET$  explained ca. 80% of the variation observed at the four sites for the 10 modeled site-years. Our work indicated that the daily  $E/ET$  decreased to a minimum value of ca. 10% for values of LAI greater than  $3 \text{ m}^2 \text{ m}^{-2}$  at the ecosystem with a dense canopy. The sensitivities of  $E/ET$  to changes in LAI increased with the decline in water and vegetation conditions at both the seasonal and the annual time scales, i.e., the variations in LAI could cause stronger effects on  $E/ET$  in the sparse-canopy ecosystems than in the dense-canopy ecosystems. It implies that the hydrological processes and vegetation productivity for ecosystems in arid environments might be more vulnerable to projected climate change than those in humid environments.

© 2009 Elsevier B.V. All rights reserved.

### 1. Introduction

Evapotranspiration (ET) is an important process for ecosystem water budgets and energy balance, and is closely linked to ecosystem productivity (Law et al., 2002; Scott et al., 2006). Vegetation transpiration ( $T$ ) and soil water evaporation ( $E$ ), controlled by different biotic and physical processes, are the two major components of ET. To accurately predict the climatic response of ecosystem functions and processes, quantifying the

partitioning of ET and its controls are critical (Williams et al., 2004; Lauenroth and Bradford, 2006). The common approaches used to partition ET currently are measurements using lysimeter, sap flow, infrared thermometers and isotopes (Evelt et al., 1994; Williams et al., 2004; Scott et al., 2006; Moran et al., 2009) and modeling (Shuttleworth and Wallace, 1985; Kustas, 1990; Brenner and Incoll, 1997; Kemp et al., 1997; Reynolds et al., 2000). Among these methods, modeling is becoming more and more popular because of its exclusive advantage in addressing ecosystem processes over a spectrum of timescales (Shugart, 2000). The Shuttleworth–Wallace model (S–W model) has been widely used for its simple and accurate consideration of hydrological processes, and good performance (Sene, 1994; Tourula and Heikinheimo, 1998; Brisson

\* Corresponding author.

E-mail address: [yugr@igsnr.ac.cn](mailto:yugr@igsnr.ac.cn) (G. Yu).

et al., 1998; Iritz et al., 1999; Anadranistakis et al., 2000; Kato et al., 2004).

Nevertheless, there are still some insufficiencies in the application of the S–W model. First, most of its applications were undertaken on croplands, with far fewer reports on its use on grasslands (Lafleur and Rouse, 1990; Nichols, 1992; Stannard, 1993). Grasslands occupy nearly 40% of global land surface and play a very important role in global energy balance and carbon budgets (White et al., 2000). In China, also about 40% of the country is covered by grasslands (Fan et al., 2008). Studies have indicated that the grassland regions in China are highly sensitive to global climate change (Ding et al., 2006). Until now very few reports have addressed the partitioning of ET in Chinese grasslands using the S–W model or other methods. The second problem is that the S–W model has mostly been used with short time periods (less than one growing season). Its long-term performance, when more processes are involved, has not been fully tested. Furthermore, due to the lack of investigating the model long-term performance, our knowledge of the partitioning of ET and its controls is critically limited. This limitation complicates our ability to predict the climatic responses of ecosystem carbon and water processes (Williams et al., 2004; Lauenroth and Bradford, 2006; Scott et al., 2006).

Many studies have indicated that  $E/ET$ , the indicator of ET partitioning, was controlled by canopy conductance at the diurnal timescale and by leaf area index (LAI) at the seasonal timescale (Sakuratani, 1987; Liu et al., 2002; Kato et al., 2004; Scott et al., 2006; Sauer et al., 2007). However, a question persists: what factor is dominantly responsible for the year-to-year and site-to-site variations? Further, due to the dearth of research on inter-site comparisons, how the effects of canopy stomatal conductance and LAI on  $E/ET$  would change across an environmental gradient remains unclear.

Using multi-year measurements of carbon and water vapor fluxes with the eddy covariance technique for four grassland ecosystems in China, we sought to address the following questions: (1) is the S–W model applicable to Chinese grasslands over long-term periods of time? (2) What is the importance of the soil water evaporation for whole ecosystem water vapor fluxes in Chinese grasslands? (3) How do the canopy stomatal conductance and LAI affect  $E/ET$  at different spatiotemporal scales? (4) How do the responses of  $E/ET$  to changes in canopy stomatal conductance and LAI vary across an environmental gradient? The ecosystems in this study belong to the main Chinese grassland types, and they illustrate an obvious water availability gradient (Fan et al., 2008), which enables us to investigate the effects of the environment over diverse spatial scales. There are obvious seasonal and inter-annual variations in ET in each ecosystem. This provides us a good opportunity to test the applicability of the S–W model.

## 2. Methods and materials

### 2.1. Study sites

Four ecosystems with distinct water availability conditions and vegetation types were selected from ChinaFLUX eddy covariance (EC) tower stations (Yu et al., 2006a,b). Shidi alpine swamp meadow (SD) is located at the Haibei alpine grassland station on the Qinghai-Tibet Plateau (37°37'N, 101°20'E; 3160 m a.s.l.). The climate at this site is characterized by strong solar radiation, with long cold winters and short cool summers. Annual mean air temperature is  $-1.7$  °C. Annual mean precipitation is 580 mm, and 80% of it falls in May–September (Yu et al., 2006a). Because the ecosystem is situated in a low-lying area, there is standing water under the canopy during the entire growing seasons. The soil is silty clay loam with a peat layer of 0.2–2 m in depth. During the peak growing seasons, the plant community reaches a height of

45 cm, maximum LAI is ca.  $4 \text{ m}^2 \text{ m}^{-2}$ , and the canopy cover is 70–80%. The dominant species are *Kobresia tibetica*, *Carex moorcroftii*, *Carex atrofusca*, *Scirpus distigmaticus*. The site is grazed by yaks and sheep only in the winter.

Gancaitan alpine shrub-meadow (GCT) is ca. 5 km away from SD (37°40'N, 101°20'E; 3293 m a.s.l.). Thus it shares the same climate conditions with SD (e.g. the mean air temperature is  $-1.7$  °C and mean annual precipitation is 580 mm). The humid climate contributes to soil moisture conditions that are favorable for plant growth. The soil is silty clay loam with a heavy clay layer of 0.1–1.0 m in depth. During the peak growing seasons, the vegetation reaches a height of about 60 cm, maximum LAI is about  $2.8 \text{ m}^2 \text{ m}^{-2}$ , and the canopy cover is 70–80%. The dominant species are *Potentilla fruticosa* (shrub species), *Kobresia capillifolia*, *Kobresia humilis*, and *Saussurea superba*. The site is also grazed by yaks and sheep only in the winter.

Damxung alpine meadow-steppe (DX) is located at the Damxung grassland station, north of Lhasa City, Tibet (30°51'N, 91°05'E; 4333 m a.s.l.). The site experiences a plateau monsoon semi-humid climate. Mean annual air temperature is  $1.3$  °C. Mean annual precipitation is 477 mm, and 80% of it falls in June–August (Yu et al., 2006a). The soil is sandy loam having a depth of 0.3–0.5 m and containing 30% of gravel, which results in low water-holding capacity and contributes to water deficit. During the peak growing seasons, the vegetation reaches a height of 5–10 cm, maximum LAI is about  $1.1 \text{ m}^2 \text{ m}^{-2}$ , and the canopy cover is 45–55%. The dominant species are *Stipa capillacea*, *Carex montis-everestii* and *Kovresia pygmaea*. The site is also grazed by yaks and sheep only in the winter.

Neimeng temperate steppe (NM) is located in Inner Mongolia, north China arid region (43°33'N, 116°40'E; 1252 m a.s.l.). The site experiences a semi-arid continental temperate climate, and precipitation is the key factor for plant growth. Mean annual temperature is  $-0.4$  °C. Mean annual precipitation is 350 mm, and more than 70% of it falls in June–August (Yu et al., 2006a). The soil is medium loam with 20% clay. During the peak growing seasons, the vegetation reaches a height of 50–60 cm, maximum LAI is about  $1.5 \text{ m}^2 \text{ m}^{-2}$ , and the canopy cover is 60–70%. The dominant species are *Leymus chinensis*, *Agropyron cristatum*, *Cleistogenes squarrosa*, and *Carex duriuscula*. The site has been fenced to prevent grazing and other disturbance since 1979, which makes the ground totally covered by the accumulated litter.

Because the instrumentation was installed at these sites at different times, the time periods investigated for this study are site-specific. For SD and GCT, the study periods extends from January 2003 to December 2005; for DX, from July 2003 to December 2005; for NM, from April 2003 to December 2004 (EC measurements at NM in 2005 were excluded because of disturbances caused by the power system). In this study, the last year's data (i.e. 2005 at SD, GCT and DX, and 2004 at NM) were used for model validation and the others were used for the calibration.

### 2.2. Measurements and data processing

Uniform open-path EC systems and meteorological instruments were installed at a height of 2.2 m and 1.5 m, respectively, to monitor  $\text{CO}_2/\text{H}_2\text{O}$  fluxes and environmental conditions over the four ecosystems. The EC system consists of an open-path  $\text{CO}_2/\text{H}_2\text{O}$  gas analyzer (model LI-7500, Licor Inc., Lincoln, Nebraska) and a 3D sonic anemometer/thermometer (model CSAT3, Campbell Scientific Inc., Logan, Utah). The signals were recorded at 10 Hz by a datalogger (Model CR5000, Campbell Scientific Inc.) and then block-averaged over 30-min intervals.

The meteorological variables, except precipitation, were measured simultaneously with the eddy fluxes and were also calculated over 30-min intervals. Net radiation ( $R_n$ ) was measured

with radiometers (Model CNR-1, Kipp & Zonnen, Delft, The Netherlands). Wind speed was measured with a cup anemometer (Model A100R, Vector Instrument, North Wales, UK). Photosynthetic active radiation (PAR) above the canopy was measured with a quantum sensor (Model LI190SB, Licor Inc.). Air temperature ( $T_a$ ) and relative humidity (RH) were measured with shielded and aspirated probes (Model HMP45C, Campbell Scientific Inc.). Vapor pressure deficit (VPD) was calculated as the difference between the saturation and actual vapor pressures at the given temperature based on the measured relative humidity and air temperature. Precipitation was recorded with a rain gauge (Model 52203, R.M. Young, Traverse City, Michigan) above the canopy. Soil temperature ( $T_s$ ) was measured using thermocouple probes (Model 105T, Campbell Scientific Inc.) at a depth of 1 cm, 5 cm, 20 cm and 40 cm, and soil volumetric water content (SW) was measured at a depth of 5 cm, 20 cm and 40 cm with TDR probes (Model CS616, Campbell Scientific Inc.). Soil heat flux ( $G$ ) was measured at the depth of 5 cm with two flux plates (Model HFP01SC, Campbell Scientific Inc.).

A three-angle coordinate rotation approach was used to align the coordinates with the mean wind (Wilczak et al., 2001), and the WPL method was used to adjust density changes resulting from fluctuations in heat and water vapor (Webb et al., 1980). The friction velocity threshold ( $u^*$ ) was empirically set as  $0.15 \text{ m s}^{-1}$  to filter measurements made under low turbulence, and the following strategies were adopted to fill the missing and rejected data (Falge et al., 2001): for small gaps (<2 h), the missing data were linearly interpolated; the missing daytime flux data were estimated as a function of PAR using the Michaelis–Menten equation with 8-day moving windows; the missing nighttime NEE, i.e., night-time ecosystem respiration ( $RE_{\text{night}}$ ) was estimated using the Van't Hoff equation; the mean diurnal variations method (MDV) was used to fill the gaps in meteorological variables. To estimate the GPP, we estimated daytime ecosystem respiration ( $RE_{\text{day}}$ ) with the relationships between the  $RE_{\text{night}}$  and soil temperature, using the Van't Hoff equation. GPP was calculated as the sum of NEE and RE. More information on the measurement systems and data processing at these sites is available in Yu et al. (2006b) and Hu et al. (2008).

Another important input variable in the S–W model is LAI. To configure integrated LAI dataset with relatively fine temporal resolution, we established a relationship between NDVI (NASA MODIS product, 8 days averaged with 1 km resolution, <http://remotesensing.ou.edu>) and the measured LAI with exponential (SD:  $y = 0.049e^{5.192x}$ ,  $R^2 = 0.93$ ; GCT:  $y = 0.011e^{6.886x}$ ,  $R^2 = 0.95$ ; NM:  $y = 0.106e^{4.064x}$ ,  $R^2 = 0.94$ ) or linear (DX:  $y = 1.983x - 0.284$ ,  $R^2 = 0.84$ ) functions and then used these functions and NDVI data to estimate the daily LAI of the entire growing seasons.

### 2.3. Modeling

The S–W model was developed based on the Penman–Monteith model (Monteith, 1965; also reproduced by Gash and Shuttleworth, 2007), which describes the water vapor flows from soil to atmosphere as being analogous to the flow of electric current. Similar to the Penman–Monteith model, the S–W model regards the canopy as one “big leaf” and thus does not consider the interactive processes taking place within the canopy. But the S–W model estimates the latent heat flux from the soil surface (i.e.  $E$ ) and from the canopy (i.e.  $T$ ) as two separate sources. There are five resistances involved in this model (Fig. 1): canopy stomatal resistance ( $r_{sc}$ ), soil surface resistance ( $r_{ss}$ ,  $\text{s m}^{-1}$ ), aerodynamic resistance of the leaf to canopy height ( $r_{ac}$ ,  $\text{s m}^{-1}$ ), resistance of the canopy height to reference height ( $r_{aa}$ ,  $\text{s m}^{-1}$ ) and soil surface to canopy height ( $r_{as}$ ,  $\text{s m}^{-1}$ ).

Through use of the S–W model, ecosystem evapotranspiration  $\lambda ET$  ( $\text{W m}^{-2}$ ) can be calculated as the sum of transpiration ( $\lambda T$ ) and

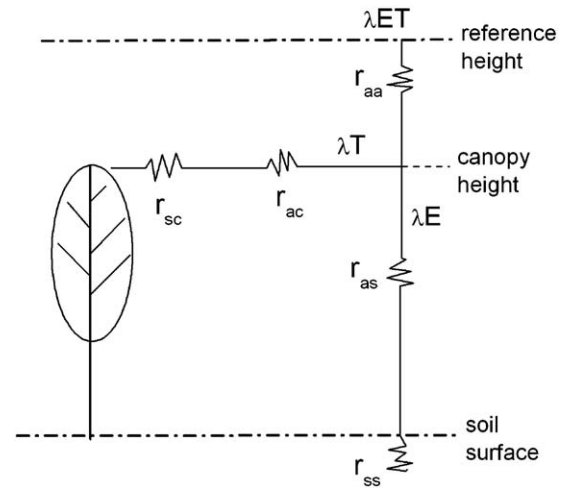


Fig. 1. Schematic description of the energy partitioning for a canopy with the S–W model.  $\lambda ET$  is the latent heat flux (i.e. evapotranspiration) from the vegetation ( $\lambda T$ ) and soil surface ( $\lambda E$ ).

soil water evaporation ( $\lambda E$ ):

$$\lambda ET = \lambda T + \lambda E = C_c PM_c + C_s PM_s \quad (1)$$

$$PM_c = \frac{\Delta R + (\rho c_p D - \Delta r_{ac} R_s) / (r_{aa} + r_{ac})}{\Delta + \gamma(1 + (r_{sc} / (r_{aa} + r_{ac})))} \quad (2)$$

$$PM_s = \frac{\Delta R + (\rho c_p D - \Delta r_{as}(R - R_s)) / (r_{aa} + r_{as})}{\Delta + \gamma(1 + (r_{ss} / (r_{aa} + r_{as})))} \quad (3)$$

where  $PM_c$  and  $PM_s$  are terms similar to that in the Penman–Monteith model to describe canopy transpiration and soil evaporation, respectively.  $C_c$  and  $C_s$  are the canopy resistance coefficient and soil surface resistance coefficient, respectively.  $\Delta$  is the slope of the saturation vapor pressure versus temperature curve ( $\text{kPa K}^{-1}$ ).  $\rho$  is the density of air ( $1.293 \text{ kg m}^{-3}$ ),  $c_p$  is the specific heat at constant pressure ( $1012 \text{ J kg}^{-1} \text{ K}^{-1}$ ),  $D$  is vapor pressure deficit ( $\text{kPa}$ ) in the air, and  $\gamma$  is the psychrometric constant ( $0.067 \text{ kPa K}^{-1}$ ). Calculations of the resistances will be addressed later. In Eqs. (2) and (3),  $R$  and  $R_s$  ( $\text{W m}^{-2}$ ) represent the available energy input above the canopy and above the soil surface, respectively, and defined as

$$R = R_n - G \quad (4)$$

$$R_s = R_{ns} - G \quad (5)$$

where  $R_n$  and  $R_{ns}$  ( $\text{W m}^{-2}$ ) are net radiation fluxes into the canopy and the substrate ( $\text{W m}^{-2}$ ), respectively.  $G$  is the soil heat flux ( $\text{W m}^{-2}$ ).  $R_{ns}$  can be estimated using Beer's law:

$$R_{ns} = R_n \exp(-0.6LAI) \quad (6)$$

In Eq. (1), the two coefficients  $C_c$  and  $C_s$  are calculated as follows:

$$C_c = \frac{1}{1 + (\rho_c \rho_a / (\rho_s (\rho_c + \rho_a)))} \quad (7)$$

$$C_s = \frac{1}{1 + (\rho_s \rho_a / (\rho_c (\rho_s + \rho_a)))} \quad (8)$$

in which  $\rho_a$ ,  $\rho_c$  and  $\rho_s$  are calculated as

$$\rho_a = (\Delta + \gamma)r_{aa} \quad (9)$$

$$\rho_c = (\Delta + \gamma)r_{ac} + \gamma r_{sc} \quad (10)$$

$$\rho_s = (\Delta + \gamma)r_{as} + \gamma r_{ss} \quad (11)$$

#### 2.4. Calculation of resistances in the S–W model

We used the same approach as Shuttleworth and Wallace (1985) to calculate the three aerodynamic resistances, i.e.,  $r_{ac}$ ,  $r_{as}$  and  $r_{aa}$  (Fig. 1). Soil surface resistance  $r_{ss}$  was estimated as the function of soil water content (Lin and Sun, 1983):

$$r_{ss} = b_1 \left( \frac{\theta_s}{\theta} \right)^{b_2} + b_3 \quad (12)$$

where  $\theta$  and  $\theta_s$  are the soil water content and saturated water content in the surface soil ( $\text{m}^3 \text{m}^{-3}$ ), and  $b_1$  ( $\text{s m}^{-1}$ ),  $b_2$ ,  $b_3$  ( $\text{s m}^{-1}$ ) are empirical constants.

Because most grassland ecosystems are located in water-limited environments and the soil water condition may have significant impact on  $r_{sc}$ , we used a modified Ball–Berry model (Ball et al., 1987; Wang and Leuning, 1998), which includes the effect of soil moisture, to estimate  $r_{sc}$

$$r_{sc} = \frac{1}{g_0 + a_1 f(\theta) P_n h_s / C_s} \quad (13)$$

$$f(\theta) = \frac{\theta - \theta_w}{\theta_f - \theta_w} \quad (14)$$

where  $g_0$  and  $a_1$  are empirical parameters,  $\theta_f$  and  $\theta_w$  are the surface soil water content (at the depth of 5 cm in this study) at field capacity and the wilting point,  $P_n$  ( $\mu\text{mol m}^{-2} \text{s}^{-1}$ ) is photosynthetic rate (GPP in this study),  $h_s$  is leaf surface relative humidity, and  $C_s$  is leaf surface  $\text{CO}_2$  content (ppm). The time step of the S–W model was set to 30-min to make it compatible with the measurements.

For the parameters in Eqs. (12)–(14),  $\theta$  was measured by the TDR probes at a depth of 5 cm,  $\theta_s$  was estimated empirically through the soil texture at each site (GCT 0.45, DX 0.35, NM 0.45),  $\theta_f$  and  $\theta_w$  were replaced with the observed maximum and minimum soil water content at the depth of 5 cm during the measurement period,  $P_n$  was replaced with GPP estimated from NEE and RE,  $h_s$  was measured by the aspirated probes (Model HMP45C, Campbell Scientific Inc.) above the canopy,  $C_s$  was replaced with the  $\text{CO}_2$  concentration above the canopy measured by the open-path  $\text{CO}_2/\text{H}_2\text{O}$  gas analyzer,  $g_0$  was assigned as a value near zero (0.00001) with the consideration that there is little or no transpiration during non-growing seasons.

$b_1$ ,  $b_2$ ,  $b_3$  and  $a_1$  were estimated through the Monte Carlo method. To minimize the uncertainty arising from the determination of the parameter ranges, the following four steps were initially taken to identify the feasible ranges of the four parameters: (1) establishing a rough range for each parameter (i.e.  $b_1$ : 1–5,  $b_2$ : 1–5,  $b_3$ : 1–1000,  $a_1$ : 1–100) with the references to Lin and Sun (1983) and Leuning (1995), (2) performing 10,000 Monte Carlo simula-

**Table 1**

Feasible ranges of parameters for each site applied to the Monte Carlo simulations.

Parameter	Range			
	SD <sup>a</sup>	GCT	DX	NM
$b_1$	–	1–5	2–5	1–5
$b_2$	–	1–4	3–5	1–3
$b_3$	40–90	150–200	1–50	450–500
$a_1$	20–50	20–50	35–65	20–50

<sup>a</sup>  $b_1$  and  $b_2$  were not estimated for SD since there was standing water under the canopy and the soil surface resistance could be regarded as a constant (i.e.  $b_3$ ).

tions with the parameter sets randomly sampled from uniform distributions within the given ranges, (3) comparing the estimated ET and the measured ET after each simulation with a linear regression function  $y = kx$ , and calculating the determinant coefficient  $R^2$  (10,000 parameter sets, and 10,000 corresponding  $k$  and  $R^2$  were obtained after this step) and (4) narrowing the parameter ranges based on the 10,000 parameter sets,  $k$ , and  $R^2$ . We selected the 200 highest  $R^2$  values under the condition that the  $k$  was in the range of 0.95–1.05. And the ranges of the distribution of the corresponding 200 parameter sets were identified as the feasible ranges. For example, the rough range of  $b_2$  was set as 1–5 at the NM site. The 200 highest  $R^2$  values were identified when  $b_2$  was distributed in the range of 1–3. Thus 1–3 was identified as the feasible range for  $b_2$  at the NM site (Table 1). As Table 1 indicates, the model performance was more sensitive to  $b_3$  and  $a_1$  than to  $b_1$  and  $b_2$ . The ranges of  $b_3$  were obviously separated among the four sites, illustrating distinct soil surface condition. The NM site had the highest  $b_3$  level, which was mainly due to the accumulated litter on the ground.

To determine the best-fit parameter set, we repeated the steps 2 and 3 above after the feasible parameter ranges had been determined. And then the 20 most successful parameter sets among the 10,000 random parameter sets were selected by applying the criteria that  $R^2$  was mostly close to one and the slope  $k$  was in the range of 0.99–1.01. We assumed that the 20 parameter sets had equal performance in modeling, and the mean of the 20 parameter sets was regarded as the best-fit parameter set (Table 2). To evaluate the accuracy in model partitioning, using the data for calibration, we calculated the ratio of the estimated  $E$  over ET ( $\sum E / \sum ET$ ) after each simulation. Based on the simulations with the 20 parameter sets, the mean and range of  $\sum E / \sum ET$  was established (Table 2). Results indicated that the two sensitive parameters  $b_3$  and  $a_1$ , and  $\sum E / \sum ET$  varied within narrow ranges, illustrating the robustness of the partitioning with the S–W model at the four ecosystems. By comparison, the performance of the S–W model during the calibration period was the best at the site GCT with a determinant coefficient near 0.9, followed by SD, NM and DX (Table 2).

**Table 2**

Range and mean (sd) of each parameter and of the ratio of total estimated  $E$  to total estimated ET ( $\sum E / \sum ET$ ) based on the simulations with the selected 20 most successful parameter sets.

Parameter and value		SD ( $R^2 > 0.8427$ )	GCT ( $R^2 > 0.8936$ )	DX ( $R^2 > 0.79963$ )	NM ( $R^2 > 0.83146$ )
$b_1$	Range	–	1.04–4.98	2.02–3.07	1.16–4.18
	Mean (sd)	–	3.04 (1.39)	2.32 (0.28)	2.63 (0.94)
$b_2$	Range	–	2.45–3.39	4.09–4.65	1.03–1.93
	Mean (sd)	–	2.84 (0.28)	4.36 (0.14)	1.32 (0.22)
$b_3$	Range	84.85–89.93	180.82–199.61	1.26–9.73	471.34–497.72
	Mean (sd)	86.91 (1.73)	193.33 (5.49)	5.35 (2.29)	486.60 (8.66)
$a_1$	Range	37.83–39.80	25.49–28.20	43.11–64.31	34.38–37.50
	Mean (sd)	38.66 (0.66)	26.55 (0.71)	54.41 (6.06)	35.85 (0.93)
$\sum E / \sum ET$ (%)	Range	59.71–60.89	56.49–60.69	55.53–65.10	63.43–66.43
	Mean (sd)	60.41 (0.40)	58.92 (1.02)	60.02 (2.69)	64.91 (0.84)

$R^2$  in the parenthesis illustrates the criterion for selecting the 20 most successful parameter sets at each site.

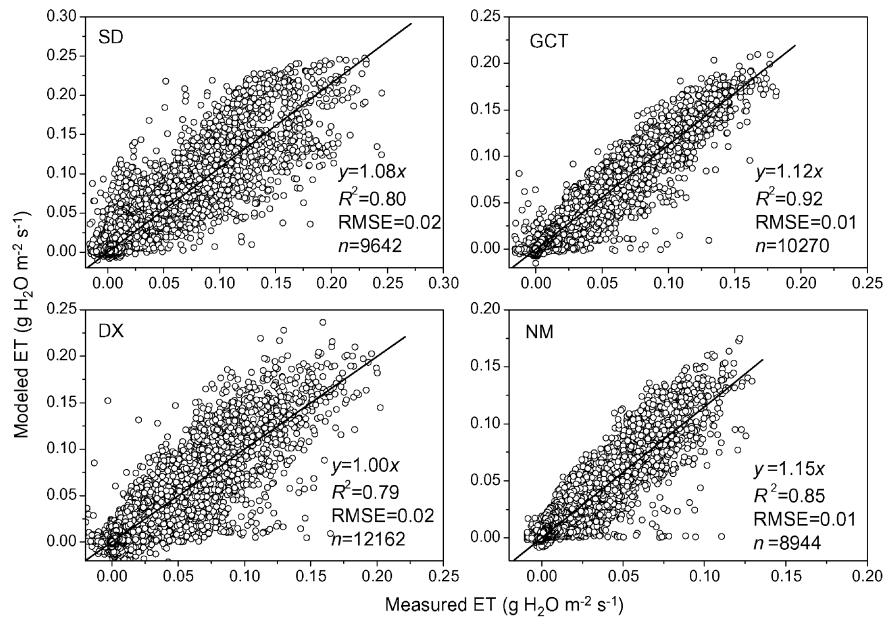


**Fig. 2.** Comparisons between the modeled and measured evapotranspiration (ET) at half-hourly time scale. The years of data used are 2005 in SD, GCT and DX and 2004 in NM. RMSE ( $\text{g H}_2\text{O m}^{-2} \text{s}^{-1}$ ) is root mean square error.

### 3. Results

#### 3.1. Performance of S–W model at the half-hour time scale

We ran the S–W model with the best parameter set which was the mean of the 20 most successful parameter sets (Table 2). In general, the model successfully simulated ET at the four ecosystems with the  $R^2$  between measured and modeled ET above 0.8 (Fig. 2). According to the slope  $k$ , the model generally overestimated ET by 8–15% at all the sites except DX. We also examined diurnal simulation in three distinct phases: pre-growing season (April), peak growing season (August) and late growing season (September). At each phase the modeled ET was in good agreement with the measurements (Fig. 3). No obvious deviation

was detected in these three phases. However, the statistical results indicated that the model performance in the growing season was better than that in non-growing season (Table 3). In addition, as Table 3 suggests, the model overestimation of ET at SD, GCT, and NM occurred mostly in the growing seasons.

#### 3.2. Performance of the S–W model at the daily time scale

The estimated ET was generally in good agreement with the measurement throughout entire years at each site (Fig. 4). There were large seasonal and day-to-day variations in ET at the four ecosystems, but they were well simulated at most times of the year. This indicates that the scheme of the S–W model and the parameterization covered the key biophysical processes of water

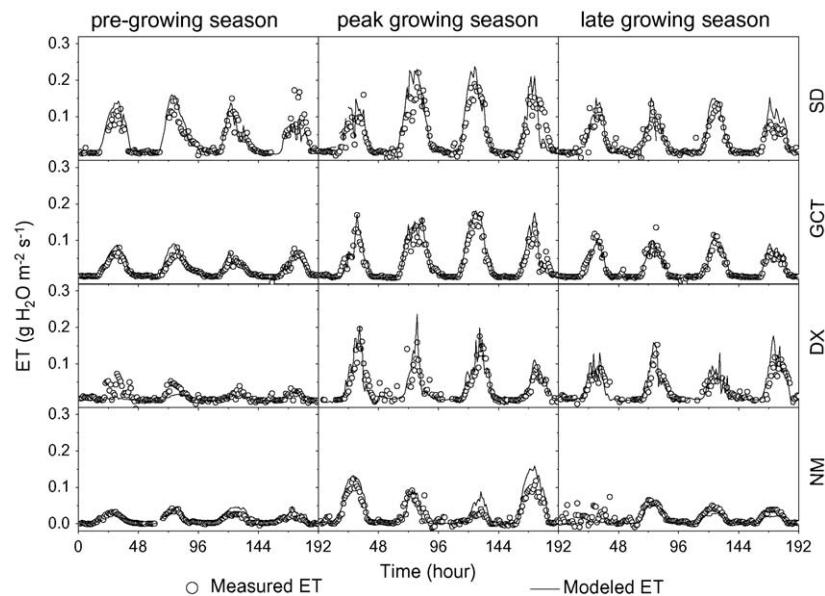


**Fig. 3.** Diurnal variations of the modeled and measured evapotranspiration (ET) during pre-growing season, peak growing season and late growing season. For the sites SD, GCT and DX, the days selected to represent each period were April 20–23, August 1–4, and September 15–18, 2005 respectively. For NM, the days selected were May 5–8 (no measured data were available in April as the result of datalogger malfunction), August 1–4 and September 15–18, 2004, respectively.

**Table 3**

Model performance in growing season and non-growing season.

Site	Growing season (May–September)				Non-growing season (October–April)			
	<i>k</i>	<i>R</i> <sup>2</sup>	RMSE	<i>n</i>	<i>k</i>	<i>R</i> <sup>2</sup>	RMSE	<i>n</i>
SD	1.10	0.82	0.03	3788	0.97	0.53	0.05	5854
GCT	1.15	0.93	0.02	4665	0.86	0.73	0.01	5605
DX	1.01	0.79	0.02	5806	0.84	0.57	0.01	6356
NM	1.15	0.84	0.01	5644	0.96	0.47	0.01	3300

**Table 4**

Performance of the S–W model at the daily time scale.

Site	All weather conditions			Rainy days rejected		
	<i>k</i>	<i>R</i> <sup>2</sup>	<i>n</i>	<i>k</i>	<i>R</i> <sup>2</sup>	<i>n</i>
SD	1.03	0.81	838	1.08	0.86	539
GCT	0.97	0.83	1066	1.05	0.91	638
DX	0.93	0.84	807	1.04	0.90	525
NM	1.06	0.85	503	1.09	0.89	405

vapor flux within the ecosystems. There was an obvious deviation between measured ET and modeled ET at DX in DOY 143–165, 2004 (Fig. 4). This disparity was mainly caused by large data gaps. During this period, about 58% of the total and 43% of daytime half-hourly EC flux data were missing. In cases with large data gaps, the quality of filled datasets would drop substantially (Falge et al., 2001).

The performance of the model at the daily time scale was summarized through statistical analysis. Considering the importance of GPP on the simulation of ET in our study (Eq. (13)), we excluded the daily data if there was gap-filled GPP between the hours of 9 and 18 (local time) during growing seasons. Furthermore, we also excluded the daily data estimated from less than 40% of robust half-hour data, including the measured ET and the input meteorological variables. The result illustrated significant linear correlations between the modeled and measured ET, with the slope *k* in the range of 0.98–1.06 and *R*<sup>2</sup> in the range of 0.81–0.85 at the four ecosystems (Table 4). When we excluded the daily ET data with rain events, there was an obvious increase of *R*<sup>2</sup> by 4–8% and of the slope *k* by 3–11%, respectively. This indicates that during rainy days, the model would system-

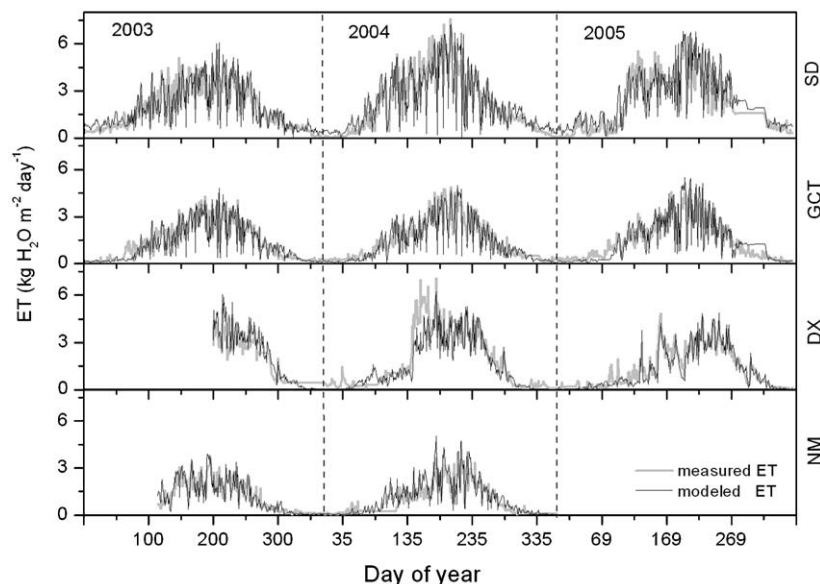
atically underestimate ET, and the ability of modeling would decrease as well.

### 3.3. Estimate of annual ET, *T* and *E*

On an annual basis, the simulated ET, *E*, *T*, and *E*/*ET* for the entire years (January–December) and for the growing seasons (May–September) were calculated (Table 5). Results indicated that the sparser the canopy, the more water would be lost from the soil surface. As the mean daily LAI decreased from 1.9 (SD) to 0.5 (DX) across ecosystems, *E*/*ET* increased from 51% to 67% for entire years and 36% to 60% for growing seasons, meaning that more than half of the water vapor flux in the entire years and more than 35% in the entire growing seasons was lost directly through the evaporation from the soil surface. During the drought conditions in 2005 at DX, the soil water accounted for as much as 67% for the whole year and 60% for the whole growing season. For ecosystems with low LAI (DX and NM), the difference between *E*/*ET* of the growing seasons and that of the entire years was near 8%. The difference, however, was doubled (16.5%) at the higher LAI sites (GCT and SD), illustrating the importance of LAI in regulating the annual ecosystem water balance.

### 3.4. Spatiotemporal dynamics of *E*/*ET* and the controlling factors

We investigated the effect of canopy stomatal conductance (*g*<sub>sc</sub>) on the diurnal variations in *E*/*ET* (modeled *E*/modeled ET) with data taken during the peak season (July 15–August 15, 2005 for SD, GCT and DX, and July 15–August 15, 2004 for NM). With the degradation of soil water condition across ecosystems, the maximum canopy stomatal conductance decreased gradually from 61.5 mm s<sup>-1</sup> (SD) to 17.4 mm s<sup>-1</sup> (NM). Consistent with

**Fig. 4.** Comparisons of the seasonal dynamics between modeled and measured evapotranspiration (ET) in 2003–2005.

**Table 5**

Magnitudes of mean daily LAI in growing seasons ( $LAI_{\text{mean}}$ ), total modeled ET ( $ET_{\text{mod}}$ ), total modeled  $E$  ( $E_{\text{mod}}$ ), total modeled  $T$  ( $T_{\text{mod}}$ ), and the ratio of  $E_{\text{mod}}$  to  $ET_{\text{mod}}$  ( $E/ET_{\text{mod}}$ ) in entire years and in growing seasons.

Site	Year	$LAI_{\text{mean}}$	All year around (January–December)				Growing season (May–September)			
			$ET_{\text{mod}}$	$E_{\text{mod}}$	$T_{\text{mod}}$	$E/ET_{\text{mod}}$	$ET_{\text{mod}}$	$E_{\text{mod}}$	$T_{\text{mod}}$	$E/ET_{\text{mod}}$
SD	2003	1.7	725	452	273	0.62	471	202	269	0.43
	2004	1.8	817	490	327	0.60	537	214	323	0.40
	2005	1.9	878	506	372	0.58	590	239	351	0.41
	Mean	1.8	807	483	324	0.60	533	218	314	0.41
GCT	2003	1.2	483	282	201	0.58	358	162	196	0.45
	2004	1.3	500	288	212	0.58	373	163	210	0.44
	2005	1.4	543	278	265	0.51	409	148	261	0.36
	Mean	1.3	509	283	226	0.56	380	158	222	0.42
DX	2004	0.5	539	333	206	0.62	453	252	201	0.56
	2005	0.5	453	303	150	0.67	361	217	144	0.60
	Mean	0.5	496	318	178	0.64	407	235	173	0.58
NM	2003	0.8	–	–	–	–	283	174	109	0.61
	2004	0.9	391	254	137	0.65	313	177	136	0.57
	Mean	0.9	–	–	–	–	298	176	123	0.59

our expectation, the canopy stomatal conductance had significant effects on the diurnal variations in  $E/ET$  at the four ecosystems ( $p < 0.001$ ) (Fig. 5).  $E/ET$  descended gradually with the increase of  $g_{\text{sc}}$  as the result of the combined effects of air humidity, PAR, soil moisture, and plant physiological rhythm. A minor increase of  $g_{\text{sc}}$  could cause substantial decrease in  $E/ET$  when  $g_{\text{sc}}$  was at a low level, but the sensitivity (i.e. the slope of the fixed curve) reduced with the increase of  $g_{\text{sc}}$ . Especially when  $g_{\text{sc}}$  exceeded  $15 \text{ mm s}^{-1}$  at the SD site,  $E/ET$  kept nearly constant (10%) without further decrease (Fig. 5).

The relationship between  $g_{\text{sc}}$  and  $E/ET$  was more scattered at DX than that at the other ecosystems, which was possibly caused by the low canopy coverage (ca. 50%). The soil water evaporation at the DX site accounted for a large fraction of ET throughout entire diurnal courses, thus the variables affecting  $E$  also play important roles in determining the diurnal variations of  $E/ET$ . For example, a significant positive relationship between  $E/ET$  and wind speed was found at this site (data not shown).

Although the swamp meadow (SD) and the shrub-meadow (GCT) were experienced the similar climate conditions, they

showed different responses of  $E/ET$  to  $g_{\text{sc}}$ .  $E/ET$  kept relatively constant when  $g_{\text{sc}}$  reached  $15 \text{ mm s}^{-1}$  at SD, illustrating no sensitivity above this threshold. But such a pattern was not detected at GCT, where  $E/ET$  could decrease obviously with the increase of  $g_{\text{sc}}$  even when  $g_{\text{sc}}$  achieved the maximum value ( $36 \text{ mm s}^{-1}$ ). This difference was mainly due to the distinct soil water conditions at the two sites. There was standing water under the canopy during the growing season at SD, causing low soil surface resistance ( $86.7 \text{ mm s}^{-1}$ ). Therefore the some water would evaporate directly from the standing water surface even if  $g_{\text{sc}}$  was very high. But the soil moisture at GCT was not saturated, and the soil surface resistance varied at high levels ( $201.2\text{--}207.1 \text{ mm s}^{-1}$ ). This resulted in persistent competition for water between the soil surface (i.e.  $E$ ) and the plant (i.e.  $T$ ). Hence the increase of  $g_{\text{sc}}$  could cause obvious decreases in  $E/ET$ . Such distinct sensitivities of  $E/ET$  to  $g_{\text{sc}}$  between SD and GCT indicate that when the soil is saturated, there is a limit for  $g_{\text{sc}}$  to regulate water evaporation from the soil surface under the canopy.

Seasonal variations in  $E/ET$  at the four ecosystems showed “one-trough” patterns throughout the study years (Fig. 6). During

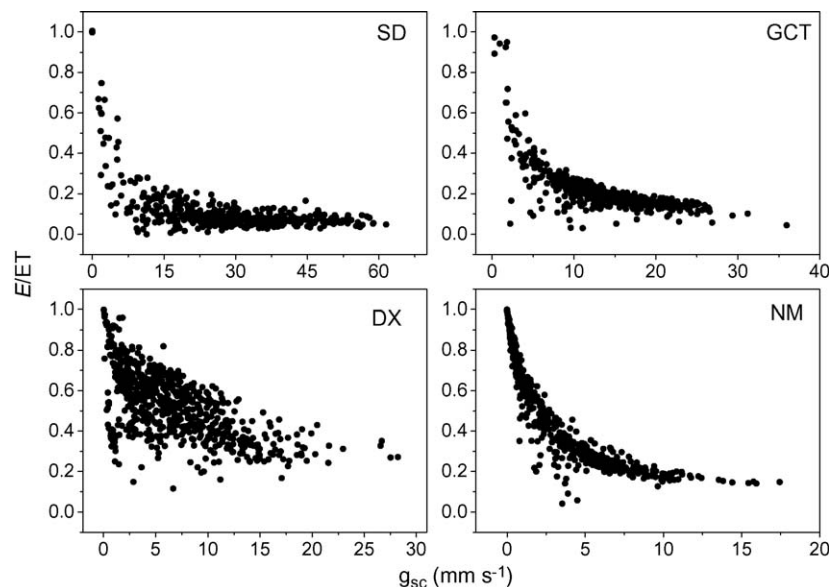


**Fig. 5.** Effect of canopy stomatal conductance ( $g_{\text{sc}}$ ) on  $E/ET$  at the half-hour time scale. Data were selected in the peak growing season (July 15–August 15) in 2005 (SD, GCT and DX) and in 2004 (NM).

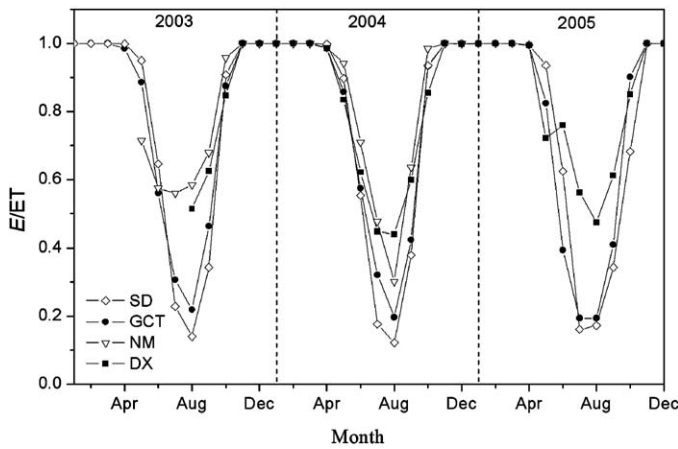


**Fig. 6.** Seasonal dynamics of the ratio of modeled monthly soil water evaporation to modeled monthly evapotranspiration ( $E/ET$ ).

the period from January to April, there was no canopy and ET was totally accounted for by  $E$  (i.e.  $E/ET = 1$ ). With the progress of growing season from May, monthly  $E/ET$  gradually decreased until the peak growing month of August. After August the monthly  $E/ET$  rose again until the end of growing season when it returned to 100%. During the years investigated, the minimum monthly  $E/ET$  was 0.12–0.16 at SD, 0.19–0.22 at GCT, 0.44–0.51 at DX and 0.30–0.56 at NM, respectively. These relatively high values indicated that soil water evaporation plays an important role in water vapor fluxes at these grasslands even in the seasons with the best canopy conditions.

The seasonal dynamics of  $E/ET$  was mainly controlled by the changes in LAI. Daily  $E/ET$  was significantly correlated with LAI (Fig. 7). When LAI was less than about  $3 \text{ m}^2 \text{ m}^{-2}$  at the SD site,  $E/ET$  decreased linearly with the increasing LAI. But when LAI exceeded this threshold, daily  $E/ET$  remained about 0.1. This is caused by the fact that  $g_{sc}$  declined when LAI exceeded  $3 \text{ m}^2 \text{ m}^{-2}$  owing to the simultaneous decrease in leaf stomatal conductance (data not shown). The slope of the fit line between LAI and  $E/ET$  was  $-0.29$  at SD,  $-0.34$  at GCT,  $-0.72$  at DX, and  $-0.49$  at NM, respectively. Such different slopes suggest that the sensitivity of  $E/ET$  to LAI increased with the decline of soil moisture and vegetation conditions. In

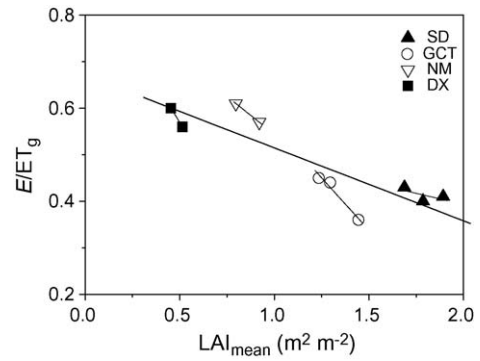


**Fig. 8.** Effect of LAI on annual  $E/ET$  at each site.  $E/ET_g$  was the ratio of modeled total  $E$  to modeled total ET in growing season, and  $LAI_{\text{mean}}$  was the mean daily LAI of each growing season.

addition, as Fig. 7 illustrates, the relationships between LAI and  $E/ET$  were more scattered in the semi-arid (NM) and semi-humid (DX) sites than those in the humid sites (SD and GCT). This is mainly because, besides LAI, the varying soil water content also affected  $E/ET$  through its influence on canopy stomatal conductance in ecosystems undertaking water deficit (data not shown).

At the annual time scale, the years with high LAI had low  $E/ET$  values (Fig. 8). According to the limited amount of yearly data in this study, the sensitivity of annual  $E/ET$  to changes in LAI tended to increase with the decline of water and vegetation, which was similar to the result at the seasonal time scale. When the four ecosystems were considered together, a spatial pattern emerged indicating that the ecosystems with high LAI had low  $E/ET$  values (Fig. 8). The regression relationships were:

$$\frac{E}{ET_g} = -0.16LAI_{\text{mean}} + 0.67 (P < 0.001, R^2 = 0.79) \quad (15)$$

$$\frac{E}{ET_g} = -0.07LAI_{\text{max}} + 0.65 (P < 0.001, R^2 = 0.75) \quad (16)$$

where  $E/ET_g$  was the ratio of total  $E$  to total ET in growing season (May–September),  $LAI_{\text{mean}}$  and  $LAI_{\text{max}}$  were the mean daily LAI and the maximum daily LAI in the growing seasons.

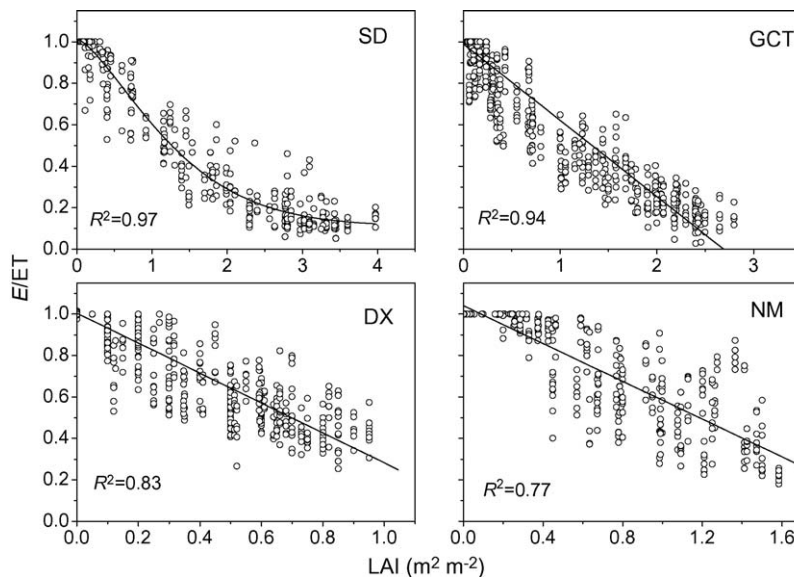


**Fig. 7.** Effect of leaf area index (LAI) on daily  $E/ET$ .  $E/ET$  was calculated as the ratio of modeled daily  $E$  to modeled daily ET.

## 4. Discussion

### 4.1. Model performance and uncertainties

The accurate estimate of ET at the diurnal and seasonal time scales in this study confirmed the ability of the S–W model to make accurate predictions for Chinese grasslands. The good performance of the S–W model was also confirmed in many other ecosystems (Tourula and Heikinheimo, 1998; Sene, 1994; Iritz et al., 1999; Kato et al., 2004). Compared with previous studies, the performance of the S–W in this study was generally better. The following three reasons may be responsible for the improvement of this study. (1) Key parameters were estimated from Monte Carlo simulations. In most previous work, key parameters were given with empirical values, which may cause large deviation due to the fact that many parameters, in most cases, are site-specific. Furthermore, the feasible parameter ranges were identified through several steps before the Monte Carlo simulations (Table 1), which could greatly reduce the uncertainty caused by the selection of parameter ranges. (2) The effect of soil water condition on canopy stomatal conductance was added to the S–W model. In most grassland ecosystems, soil moisture is the main limiting factor for the plant physiological processes. Taking this into account could result in improvement in the model. (3) Robust EC data were used for the model–measurement comparison, which largely reduced the uncertainty arising from the deficiency of measurement method (Baldocchi et al., 2001). Although there was no direct measurement of  $E$  or  $T$  to test the accuracy of partitioning, the conservative  $E/ET$  based on the simulations with the 20 most successful parameter sets enhanced our confidence in the performance of the model (Table 2).

The parameters in the S–W model of this study were fixed for each ecosystem throughout the periods investigated, which probably accounts for the systematic overestimation of ET for some ecosystems in the growing seasons (Table 3). Studies have suggested that there may be great seasonal and inter-annual variations in some parameters (e.g.  $a_1$  in Eq. (13)) due to the changes in environmental and vegetation conditions (Wever et al., 2002; Winkel et al., 2001). To explore this issue, also by conducting the Monte Carlo simulations, we estimated the parameters only with data for validation (e.g. 2004 for the NM site). The results illustrated that the model performance was obviously improved, with slope  $k$  of the relationship between the measured and modeled ET getting much closer to 1 (1.00 at SD, 1.03 at GCT and 1.04 at NM) without sacrificing the  $R^2$  and the accuracy of the partitioning. But the value of  $a_1$  changed from 20 to 39 at SD, 27 to 21 at GCT, and 36 to 27 at NM. Meanwhile  $E/ET$  was not strongly affected by the “new” parameter sets. For example, at the NM site the regression correlation between the  $E/ET$  based on the “old” parameter set ( $b_1 = 2.63$ ,  $b_2 = 1.32$ ,  $b_3 = 486.6$ ,  $a_1 = 35.85$ , Table 2) and on the “new” parameter set ( $b_1 = 1.83$ ,  $b_2 = 2.12$ ,  $b_3 = 493.8$ ,  $a_1 = 27.42$ ) was extremely significant ( $R^2 = 0.99$ ,  $k = 0.99$ ,  $p < 0.001$ ).

In this study, the S–W model only concerned the water vapor flux from the soil water evaporation and transpiration without considering direct evaporation from the canopy. On rainy days, the canopy interception may account for a considerable fraction of the total ET. As Table 2 shows, on rainy days the modeled ET was obviously lower than measured value. Tourula and Heikinheimo (1998) estimated the water balance for a barley crop (maximum LAI 3.5–4.5  $\text{m}^2 \text{m}^{-2}$ ). They found that the interception accounted for 9–14% of the total ET. Although the canopies in this study are not as dense as the barley crop, interception may also account for a certain amount of ET. In addition, it is acknowledged the model performance in the non-growing seasons was not as satisfactory as that in the growing seasons. Further study is needed to address this issue.

### 4.2. Variations of $E/ET$ and controlling factors

The magnitudes and ranges of variations in  $E/ET$  in this study were consistent with previous studies. The monthly  $E/ET$  of the peak growing seasons (August) at SD was 0.12–0.16, and the daily  $E/ET$  remained about 0.1 when LAI was higher than 3  $\text{m}^2 \text{m}^{-2}$ . Similarly, Liu et al. (2002) estimated  $E/ET$  over a winter wheat and summer maize crop through measurements by lysimeter in north China. They found the monthly  $E/ET$  was near 0.2 in peak growing seasons. The study of Sakuratani (1987) also demonstrated daily  $E/ET$  was very close to 0.1 when LAI reached 3  $\text{m}^2 \text{m}^{-2}$ . Sauer et al. (2007) investigated the allocation of water vapor flux over a soybean crop, they also found daily  $E/ET$  was about 0.08 when the canopy became close (LAI > 5  $\text{m}^2 \text{m}^{-2}$ ). With EC and sap-flow measurements, Scott et al. (2006) investigated the seasonal dynamics of  $E/ET$  over a desert shrub-grassland ecosystem (vegetation height 0.3–1 m, vegetation cover 51%). Their results indicated that monthly  $E/ET$  was about 0.3 during the peak growing season. At the shrub-grassland site (GCT) in our study, the vegetation condition was better and  $E/ET$  (0.19–0.22) was a bit lower. Reynolds et al. (2000) simulated the evapotranspiration in two communities in the Chihuahuan desert over 100-year period (mean annual precipitation 230 mm), finding the mean annual  $E/ET$  for the two arid communities was ca. 0.66. Similarly, Lauenroth and Bradford (2006) analyzed the water budget of a temperate short-grass steppe in Colorado over 39 years (mean annual precipitation 340 mm). Their results show that the annual  $E/ET$  ranged from 0.25 to 0.6 with the average of 0.49. It seems like that  $E/ET$  in the temperate steppe site NM (0.65) is a bit higher than the sites of Reynolds et al. (2000) and Lauenroth and Bradford (2006) according its precipitation condition (mean annual precipitation 350 mm).

Unexpectedly, despite the large amount of litter covering the soil surface at the NM site, which caused the high basic soil surface resistance ( $b_3$  in Table 2),  $E/ET$  was not obviously different from that measured at the other sites. This may be because plants at this site were conservative in using soil water and the canopy conductance remained at a very low level, which constrained water loss through transpiration.

In terms of the mechanisms controlling  $E/ET$ , our results highlighted the importance of the biotic factors, i.e., the canopy stomatal conductance and LAI. Canopy stomatal conductance controlled  $E/ET$  at the diurnal timescale. And the variations and magnitude of LAI explained most of the seasonal, annual and site-to-site variations in  $E/ET$ . Many studies on crops found the relationship between  $E/ET$  and LAI could be described with logarithmic functions, which meant  $E/ET$  reduced gradually with the increase of LAI and finally approached a constant value (Liu et al., 2002; Kato et al., 2004). Only SD had a similar pattern in this study (Fig. 7). We conclude that this result occurred because the maximum LAI at the other grassland ecosystems was not high enough. The ability of LAI to explain variation in  $E/ET$  was weaker for the arid ecosystems than for the humid ecosystems (Fig. 7), illustrating a shift of factors from LAI to soil water content in controlling the seasonal variation of  $E/ET$  with the increase of aridity. Similarly, Liu et al. (2002) also found  $E/ET$  was jointly controlled by LAI of the crop communities and soil moisture when soil moisture became the limiting factor.

In practice, it is difficult to estimate  $E/ET$  at regional or global scales because of the lack of detailed data. The significant spatial correlation between LAI and  $E/ET$  (Eqs. (15) and (16)) suggests that it may be feasible to evaluate the partitioning of ecosystem ET in grasslands simply using the LAI data, which can be easily acquired through the remote sensing images.

Across the ecosystems, the sensitivity of  $E/ET$  in response to variations in LAI increased with the decline of water and vegetation at both the seasonal and annual time scales (Figs. 7 and 8). This

trend was likely due to the interactions between the various mechanisms through which LAI affects  $E/ET$ . As the structure of the S–W model demonstrates (Fig. 1), LAI can improve  $E/ET$  through three mechanisms: by promoting canopy stomatal resistance, by promoting aerodynamic resistance of the soil surface to canopy height ( $r_{as}$ ), and by reducing the energy input into the soil surface ( $R_{ns}$ ). All the three mechanisms work together at the sites with sparse vegetations, and  $E/ET$  shows a highly sensitive response to changes in LAI. But with the improvement of canopy conditions, the effects of the latter two mechanisms would weaken owing to the nonlinear response of  $r_{as}$  and  $R_{ns}$  to LAI (Eq. (6)), which results in the decreasing sensitivities of  $E/ET$  to LAI. This implies that variations in environmental factors, which directly determine changes in LAI, may have more significant effect on the hydrological processes and productivity in arid ecosystems than that in humid ecosystems.

## 5. Conclusion

With multi-year measurements of ecosystem evapotranspiration with eddy covariance systems, this study confirmed the good long-term performance of the S–W model at the four grassland ecosystems in China. Our study indicates that taking into account canopy rainfall interception and using varied parameter sets in different years may improve the model performance. The results of this study highlight the importance of soil water evaporation in water vapor fluxes for Chinese grasslands, and future work should pay attention to the role of soil water evaporation in terms of ecosystem carbon and water cycles. Canopy stomatal conductance and LAI are the dominant factors controlling the variations in  $E/ET$  at different spatiotemporal scales, suggesting that the climate change-induced biotic variations may have stronger impacts on the partitioning of ET than the direct effects for these vegetation communities. The different sensitivities of  $E/ET$  to LAI under different environment and vegetation conditions suggest that the hydrological processes and vegetation productivity for ecosystems in arid environments might be more vulnerable to projected climate change, and thus it would be more important to conserve the ecosystems in arid environment from the perspective of high water use efficiency.

## Acknowledgements

This research was jointly funded by National Natural Science Foundation of China (Grant Nos. 30590381, 30800151 and 30700110), the Knowledge Innovation Program of the Chinese Academy of Sciences (Grant No. KZCX2-YW-432), the National Key Research and Development Program (Grant No. G2002CB412501), and the “Hundred Talents” Program of the Chinese Academy of Sciences. We thank two anonymous reviewers for their valuable comments to improve this manuscript. Special thanks to Mr. David C. Brill at the University of Tennessee and Dr. John H.C. Gash for revising the English writing of our manuscript.

## References

- Anadranistakis, M., Liakatas, A., Kerkides, P., Rizos, S., Gavanosis, J., Poulouvassilis, A., 2000. Crop water requirements model tested for crops grown in Greece. *Agricultural Water Management* 45 (3), 297–316.
- Ball, J.T., Woodrow, I.E., Berry, J.A., 1987. A model predicting stomatal conductance and its contribution to the control of photosynthesis under different environmental conditions. In: Biggens, I. (Ed.), *Progress in Photosynthesis Research*. Martinus-Nijhoff Publishers, Dordrecht, The Netherlands, pp. 221–224.
- Baldocchi, D., Falge, E., Gu, L.H., Olson, R., Hollinger, D., Running, S., Anthoni, P., Bernhofer, C., Davis, K., Evans, R., Fuentes, J., Goldstein, A., Katul, G., Law, B., Lee, X.H., Malhi, Y., Meyers, T., Munger, W., Oechel, W., Paw, U.K.T., Pilegaard, K., Schmid, H.P., Valentini, R., Verma, S., Vesala, T., Wilson, K., Wofsy, S., 2001. FLUXNET: a new tool to study the temporal and spatial variability of ecosystem-scale carbon dioxide, water vapor, and energy flux densities. *Bulletin of the American Meteorological Society* 82 (11), 2415–2434.
- Brenner, A.J., Incoll, L.D., 1997. The effect of clumping and stomatal response on evaporation from sparsely vegetated shrublands. *Agricultural and Forest Meteorology* 84 (3–4), 187–205.
- Brisson, N., Itier, B., L’Hotel, J.C., Lorendeau, J.Y., 1998. Parameterization of the Shuttleworth–Wallace model to estimate daily maximum transpiration for use in crop models. *Ecological Modelling* 107 (2–3), 159–169.
- Ding, Y.H., Ren, G.Y., Shi, G.Y., Gong, P., Zheng, X.H., Zhai, P.M., Zhang, D.E., Zhao, Z.C., Wang, S.W., Wang, H.J., Luo, Y., Chen, D.L., Gao, X.J., Dai, X.S., 2006. National assessment report of climate change. I Climate change in China and its future trend. *Advances in Climate Change Research* 2 (1), 3–8 (in Chinese).
- Evett, S.R., Matthias, A.D., Warrick, A.W., 1994. Energy-balance model of spatially-variable evaporation from bare soil. *Soil Science Society of America Journal* 58 (6), 1604–1611.
- Falge, E., Baldocchi, D., Olson, R., Anthoni, P., Aubinet, M., Bernhofer, C., Burba, G., Ceulemans, R., Clement, R., Dolman, H., Granier, A., Gross, P., Grünwald, T., Hollinger, D., Jensen, N.O., Katul, G., Kerönen, P., Kowalski, A., Chun, T.L., Law, B., Meyers, T., Moncrieff, J., Moors, E., Munger, J.W., Pilegaard, K., Rannik, Ü., Rebmann, C., Suyker, A., Tenhunen, J., Tu, K., Verma, S., Vesala, T., Wilson, K., Wofsy, S., 2001. Gap filling strategies for defensible annual sums of net ecosystem exchange. *Agricultural and Forest Meteorology* 107 (1), 43–69.
- Fan, J.W., Zhong, H.P., Harris, W., Yu, G.R., Wang, S.Q., Hu, Z.M., Yue, Y.Z., 2008. Carbon storage in the grasslands of China based on field measurements of above- and below-ground biomass. *Climatic Change* 86 (3–4), 375–396.
- Gash, J.H.C., Shuttleworth, W.J., 2007. *Benchmark Papers in Hydrology: Evaporation*. IAHS Press, Wallingford, p. 521.
- Hu, Z.M., Yu, G.R., Fu, Y.L., Sun, X.M., Li, Y.N., Shi, P.L., Wang, Y.F., Zheng, Z.M., 2008. Effects of vegetation control on ecosystem water use efficiency within and among four grassland ecosystems in China. *Global Change Biology* 14 (7), 1609–1619.
- Iritz, Z., Lindroth, A., Heikinheimo, M., Grelle, A., Kellner, E., 1999. Test of a modified Shuttleworth–Wallace estimate of boreal forest evaporation. *Agricultural and Forest Meteorology* 98–99, 605–619.
- Kato, T., Kimura, R., Kamichika, M., 2004. Estimation of evapotranspiration, transpiration ratio and water-use efficiency from a sparse canopy using a compartment model. *Agricultural Water Management* 65 (3), 173–191.
- Kemp, P.R., Reynolds, J.F., Pachepsky, Y., Chen, J., 1997. A comparative modeling study of soil water dynamics in a desert ecosystem. *Water Resources Research* 33, 73–90.
- Kustas, W.P., 1990. Estimates of evaporation with a one- and two-layer model of heat transfer over partial canopy cover. *Journal of Applied Meteorology* 29, 704–715.
- Lafleur, P.M., Rouse, W.R., 1990. Application of an energy combination model for evaporation from sparse canopies. *Agricultural and Forest Meteorology* 49, 135–153.
- Lauenroth, W.K., Bradford, J.B., 2006. Ecohydrology and the partitioning AET between transpiration and evaporation in a semiarid steppe. *Ecosystems* 9 (5), 756–767.
- Law, B.E., Falge, E., Gu, L., Baldocchi, D., Bakwin, P., Berbigier, P., Davis, K., Dolman, A.J., Falk, M., Fuentes, J.D., Goldstein, A., Granier, A., Grelle, A., Hollinger, D., Janssens, I.A., Jarvis, P., Jensen, N.O., Katul, G., Malhi, Y., Matteucci, G., Meyers, T., Monson, R., Munger, W., Oechel, W., Olson, R., Pilegaard, K., Paw, U.K.T., Thorgeirsson, H., Valentini, R., Verma, S., Vesala, T., Wilson, K., Wofsy, S., 2002. Environmental controls over carbon dioxide and water vapor exchange of terrestrial vegetation. *Agricultural and Forest Meteorology* 113 (1–4), 97–120.
- Leuning, R., 1995. A critical appraisal of a combined stomatal-photosynthesis model for  $C_3$  plants. *Plant Cell and Environment* 18 (4), 339–355.
- Lin, J.D., Sun, S.E., 1983. Moisture and heat flow in soil and their effects on bare soil evaporation. *Trans. Water Conservancy* 7, 1–7 (in Chinese).
- Liu, C.M., Zhang, X.Y., Zhang, Y.Q., 2002. Determination of daily evaporation and evapotranspiration of winter wheat and maize by large-scale weighing lysimeter and micro-lysimeter. *Agricultural and Forest Meteorology* 111 (2), 109–120.
- Monteith, J.L., 1965. Evaporation and environment. *Symposia of the Society for Experimental Biology* 19, 205–234.
- Moran, M.S., Scott, R.L., Keefer, T.O., Emmerich, W.E., Hernandez, M., Nearing, G.S., Paige, G.B., Cosh, M.H., O’Neill, P.E., 2009. Partitioning evapotranspiration in semiarid grassland and shrubland ecosystems using time series of soil surface temperature. *Agricultural and Forest Meteorology* 149 (1), 59–72.
- Nichols, W.D., 1992. Energy budgets and resistances to energy-transport in sparsely vegetated rangeland. *Agricultural and Forest Meteorology* 60 (3–4), 221–247.
- Reynolds, J.F., Kemp, P.R., Tenhunen, J.D., 2000. Effects of long-term rainfall variability on evapotranspiration and soil water distribution in the Chihuahuan Desert: A modeling analysis. *Plant Ecology* 150 (1–2), 145–159.
- Sakuratani, T., 1987. Studies on evapotranspiration from crops. 2. Separate estimation of transpiration and evaporation from a soybean field without water shortage. *Journal of Agricultural Meteorology* 42, 309–317.
- Sauer, T.J., Singer, J.W., Prueger, J.H., DeSutter, T.M., Hatfield, J.L., 2007. Radiation balance and evaporation partitioning in a narrow-row soybean canopy. *Agricultural and Forest Meteorology* 145 (3–4), 206–214.
- Scott, R.L., Huxman, T.E., Cable, W.L., Emmerich, W.E., 2006. Partitioning of evapotranspiration and its relation to carbon dioxide exchange in a Chihuahuan Desert shrubland. *Hydrological Processes* 20 (15), 3227–3243.

- Sene, K.J., 1994. Parameterizations for energy transfers from a sparse vine crop. *Agricultural and Forest Meteorology* 71 (1–2), 1–18.
- Shugart, H.H., 2000. Ecosystem modeling. In: Sala, O.E., Jackson, R.B., Mooney, H.A., Howarth, R.W. (Eds.), *Methods in Ecosystem Science*. Springer, New York, pp. 373–388.
- Shuttleworth, W.J., Wallace, J.S., 1985. Evaporation from sparse crops—an energy combination theory. *Q.J. Royal Meteorological Society* 111, 839–855.
- Stannard, D.I., 1993. Comparison of Penman–Monteith, Shuttleworth–Wallace, and modified Priestley–Taylor evapotranspiration models for wildland vegetation in semiarid rangeland. *Water Resources Research* 29 (5), 1379–1392.
- Tourula, T., Heikinheimo, M., 1998. Modelling evapotranspiration from a barley field over the growing season. *Agricultural and Forest Meteorology* 91 (3–4), 237–250.
- Wang, Y.P., Leuning, R., 1998. A two-leaf model for canopy conductance, photosynthesis and partitioning of available energy. I. Model description and comparison with a multi-layered model. *Agricultural and Forest Meteorology* 91 (1–2), 89–111.
- Webb, E.K., Pearman, G.I., Leuning, R., 1980. Correction of flux measurement for density effects due to heat and water vapor transfer. *Q.J. Royal Meteorological Society* 106, 85–100.
- Wever, L.A., Flanagan, L.B., Carlson, P.J., 2002. Seasonal and interannual variation in evapotranspiration, energy balance and surface conductance in a northern temperate grassland. *Agricultural and Forest Meteorology* 112 (1), 31–49.
- White, R., Murray, S., Rohweder, M., 2000. Pilot Analysis of Global Ecosystems (PAGE): Grassland Ecosystems. World Resources Institute, Washington, DC.
- Wilczak, J.M., Oncley, S.P., Stage, S.A., 2001. Sonic anemometer tilt correction algorithms. *Boundary-Layer Meteorology* 99 (1), 127–150.
- Williams, D.G., Cable, W., Hultine, K., Hoedjes, J.C.B., Yezpe, E.A., Simonneaux, V., Er-Raki, S., Boulet, G., de Bruin, H.A.R., Chehbouni, A., Hartogensis, O.K., Timouk, F., 2004. Evapotranspiration components determined by stable isotope, sap flow and eddy covariance techniques. *Agricultural and Forest Meteorology* 125 (3–4), 241–258.
- Winkel, T., Payne, W., Renno, J.F., 2001. Ontogeny modifies the effects of water stress on stomatal control, leaf area duration and biomass partitioning of *Pennisetum glaucum*. *New Phytologist* 149 (1), 71–82.
- Yu, G.R., Fu, Y.L., Sun, X.M., Wen, X.F., Zhang, L.M., 2006a. Recent progress and future directions of ChinaFLUX. *Science in China Series D: Earth Sciences* 49, 1–23.
- Yu, G.R., Wen, X.F., Sun, X.M., Tanner, B.D., Lee, X.H., Chen, J.Y., 2006b. Overview of ChinaFLUX and evaluation of its eddy covariance measurement. *Agricultural and Forest Meteorology* 137 (3–4), 125–137.